J|A|C|S ARTICLES

Published on Web 08/10/2009

Growth Patterns and Shape Development of Zeolite Nanocrystals in Confined Syntheses

Won Cheol Yoo,[†] Sandeep Kumar,[‡] R. Lee Penn,[†] Michael Tsapatsis,[‡] and Andreas Stein*,[†]

Departments of Chemistry and Chemical Engineering & Materials Science, University of Minnesota, Minneapolis, Minnesota 55455

Received June 2, 2009; E-mail: a-stein@umn.edu

Abstract: The effects of confinement on the morphological development of the zeolite silicalite-1 were studied during hydrothermal synthesis in three-dimensionally ordered macroporous (3DOM) carbon monoliths. By scheduling multiple infiltration/hydrothermal reaction (IHT) steps using precursor solutions with high (H) or low nutrient content (L) in specific sequences, it was possible to obtain various zeolite morphologies of interest for technological applications. The special morphologies are also functions of shaping and templating effects by the 3DOM carbon reactor and functions of limited mass transport in the confined reaction environment. IHT steps employing high nutrient concentrations favor nucleation, whereas those using low nutrient concentrations provide growth-dominant conditions. Observed product morphologies include polycrystalline sphere arrays for the sequence HHH..., single crystal domains spanning dozens of macropores for the sequence LLL..., and faceted silicalite-1 crystallites with dimensions less than 100 nm with the sequence HLLL.... Most of these crystallites have dimensions less than 100 nm and would be suitable building blocks for seeded zeolite membrane growth. Finally, the sequence LLL...H introduces a secondary population of particles with smaller size, so that the size distribution of zeolite crystallites in the combined population may be tuned, for example, to optimize packing of particles. Hence, by choosing the appropriate infiltration program, it is possible to control grain sizes in polycrystalline particles (spheres and opaline arrays of spheres), which alters the concentration of grain boundaries in the particles and is expected to influence transport properties through the zeolite.

Introduction

In many applications, the properties of particles depend on particle size and dispersity,[1,2] as well as morphological features, including isotropic versus anisotropic shapes, aspect ratios,[3,4] surface regularity, and surface areas.[5−7] In the case of hydrothermally prepared zeolites, for example, particle size influences the diffusion of reagents through the micropore system, the surface area impacts access to the micropore system, and particle shapes/aspect ratios affect packing of zeolite particles, for example, when they are used as seed layers to prepare membranes by secondary growth. Ways of controlling the size and shape of zeolite particles have been investigated intensively. In the late 1980s and early 1990s, much research focused on growing large single crystals of zeolites, but in more recent years, attention has also turned to zeolite nanoparticles.[8,9] Larger zeolite crystals are typically prepared by the addition of nucleation suppressors,[10,11] whereas very small crystallites are synthesized by providing conditions that favor nucleation while carefully controlling the reaction stoichiometry, crystallization time, and temperature.[12−15] Because particle growth has to be suppressed in nanozeolite syntheses, yields are often low.

Recently, various approaches to zeolite synthesis in confinement have been described, which can provide better control over sizes and shapes of zeolite particles than conventional hydrothermal syntheses.[12,16−26] A porous template can be used to

[†] Department of Chemistry.
[‡] Department of Chemical Engineering & Materials Science.

(1) Peng, X.; Wickham, J.; Alivisatos, A. P. *J. Am. Chem. Soc.* **1998**, *120*, 5343–5344.
(2) Yin, Y.; Alivisatos, A. P. *Nature* **2005**, *437*, 664–670.
(3) Jun, Y.-W.; Choi, J.-S.; Cheon, J. *Angew. Chem., Int. Ed.* **2006**, *45*, 3414–3439.
(4) Xia, Y.; Xiong, Y.; Lim, B.; Skrabalak, S. E. *Angew. Chem., Int. Ed.* **2009**, *48*, 60–103.
(5) Tao, Y.; Kanoh, H.; Abrams, L.; Kaneko, K. *Chem. Rev.* **2006**, *106*, 896–910.
(6) Corma, A. *Chem. Rev.* **1997**, *97*, 2373–2419.
(7) Pérez-Ramírez, J.; Christensen, C. H.; Egeblad, K.; Christensen, C. H.; Groen, J. C. *Chem. Soc. Rev.* **2008**, *37*, 2530–2542.
(8) Snyder, M. A.; Tsapatsis, M. *Angew. Chem., Int. Ed.* **2007**, *46*, 7560–7573.
(9) Drews, T. O.; Tsaptsis, M. *Curr. Opin. Colloid Interface Sci.* **2005**, *10*, 233–238.
(10) Qiu, S.; Yu, J.; Zhu, G.; Terasaki, O.; Nozue, Y.; Pang, W.; Xu, R. *Microporous Mesoporous Mater.* **1998**, *21*, 245–251.
(11) Lethbridge, Z. A. D.; Williams, J. J.; Walton, R. I.; Evans, K. E.; Smith, C. W. *Microporous Mesoporous Mater.* **2005**, *79*, 339–352.
(12) Tosheva, L.; Valtchev, V. P. *Chem. Mater.* **2005**, *17*, 2494–2513.
(13) Schoeman, B. J.; Sterte, J.; Otterstedt, J.-E. *Zeolites* **1994**, *14*, 110–116.
(14) Yamamura, M.; Chaki, K.; Wakatsuki, T.; Okado, H. *Zeolites* **1994**, *14*, 643–649.
(15) Mintova, S.; Bein, T. *Adv. Mater.* **2001**, *13*, 1880–1883.
(16) Holland, B. T.; Abrams, L.; Stein, A. *J. Am. Chem. Soc.* **1999**, *121*, 4308–4309.
(17) Madsen, C.; Jacobsen, C. J. H. *Chem. Commun.* **1999**, 673–674.
(18) Zhang, B.; Davis, S. A.; Mendelson, N. H.; Mann, S. *Chem. Commun.* **2000**, 781–782.

Scheme 1. Illustration of Different Zeolite Growth Patterns Obtained by Programming Sequences of IHT Cycles with Selected Nutrient Concentrations in the Precursor That Penetrates the 3DOM Carbon Reactor[a]

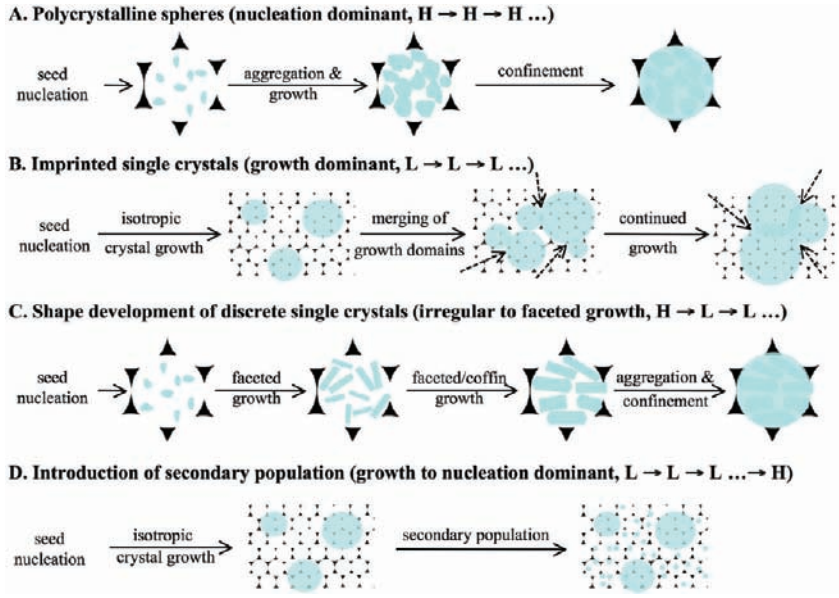

[a] L = low nutrient concentration, H = high nutrient concentration. (A) Growth of polycrystalline spheres in a sequence where nucleation dominates during each step. (B) Single crystal growth in a system where the low nutrient concentration favors slow growth. The blue circles represent single crystal domains formed after several L cycles and spanning multiple macropores, and the dashed black arrows indicate regions of merging domains. (C) Shape development from discrete, irregular seeds precipitated during an H step to faceted, coffin-shaped zeolite particles after changing to L steps to switch from nucleation to growth dominant conditions. (D) A secondary population of smaller zeolite particles results from a change of solutions that switch from growth to nucleation dominant conditions. The size of the templating macropores is the same in all cases.

either define the size of zeolite particles or to introduce extra voids into the particles.[22,25] One promising approach involves syntheses in porous carbon reactors with close-packed arrays of mesopores (3DOm carbon) or macropores (3DOM carbon) that are interconnected in three dimensions. Porous carbon is chemically and thermally stable under the conditions used in hydrothermal zeolite syntheses and can be removed from the product by simple calcination in air. 3DOm carbon was recently used to prepare colloidal crystals of 10−40 nm silicalite-1 spheres by steam-assisted crystallization of a templated amorphous precursor.[25] This method enabled syntheses of uniform and isolatable nanocrystals, as well as single-crystal zeolites with ordered, imprinted mesoporosity. 3DOM carbon reactors with larger pores (100−350 nm) were found to be suitable for hydrothermal syntheses of filled or hollow polycrystalline zeolite spheres.[26] In these syntheses, the macroscopic structure depended on the interplay between the charge on the 3DOM carbon surface and the surface charge of the product particles. It also varied according to the position within the monolithic 3DOM carbon host. The study briefly reported that lowering the silica concentration of the precursor resulted in "crystal shapes that were influenced both by the atomic crystal structure of the zeolite and by confinement effects."[26] The microstructure and the degree of crystallinity of these products had not been investigated at that time.

Here, we build on the concept of hydrothermal zeolite syntheses in the confinement of monolithic 3DOM carbon reactors and illustrate that by carrying out multiple infiltration/hydrothermal reaction (IHT) steps using specified sequences of precursor concentrations, it is possible to influence the growth pattern and shape development of zeolites and significantly enhance the control over crystal morphology. Depending on the IHT schedule, it is possible to move beyond the polycrystalline spheres reported earlier and synthesize single crystalline spheres, single crystalline arrays of spheres with hierarchical pore structure, polycrystalline spheres with tunable single crystal grain sizes, small faceted zeolite particles (<100 nm in length) in relatively high yield (i.e., virtually every reactor cage occupied with multiple crystallites), and mixed populations of zeolite particles with controllable size distributions.

The concept of scheduled multistep syntheses to control product morphology is illustrated in Scheme 1. The syntheses studied here involve two silica precursor solutions with different nutrient concentrations. The "low concentration" precursor (L) contains a component ratio of 10 SiO_2/4.5 tetrapropylammonium hydroxide (TPAOH)/4750 H_2O and the "high concentration" solution (H) a ratio of 10 SiO_2/2.4 TPAOH/0.87 NaOH/114 H_2O. The other parameters were the same for each set of conditions, except for the duration of each IHT cycle: 2 days for each H_n step and 4 days each L_n step to observe significant changes in a reasonable amount of time (note: the subscript n refers to the IHT cycle number using the corresponding precursor, H or L). Precursor H favors nucleation, and even when crystals grow in later H steps in a sequence, additional

(19) Schmidt, I.; Madsen, C.; Jacobsen, C. J. H. *Inorg. Chem.* **2000**, *39*, 2279–2283.
(20) Jacobsen, C. J. H.; Madsen, C.; Janssens, T. V. W.; Jakobsen, H. J.; Skibsted, J. *Microporous Mesoporous Mater.* **2000**, *39*, 393–401.
(21) Dong, A.; Wang, Y.; Tang, Y.; Zhang, Y.; Ren, N.; Gao, Z. *Adv. Mater.* **2002**, *14*, 1506–1510.
(22) Kim, S.-S.; Shah, J.; Pinnavaia, T. J. *Chem. Mater.* **2003**, *15*, 1664–1668.
(23) Chem, Z.; Li, S.; Yan, Y. *Chem. Mater.* **2005**, *17*, 2262–2266.
(24) Wang, J.; Vinu, A.; Coppens, M.-O. *J. Mater. Chem.* **2007**, *17*, 4265–4273.
(25) Fan, W.; Snyder, M. A.; Kumar, S.; Lee, P.-S.; Yoo, W. C.; McCormick, A. V.; Penn, R. L.; Stein, A.; Tsapatsis, M. *Nat. Mater.* **2008**, *7*, 984–991.
(26) Yoo, W. C.; Kumar, S.; Wang, Z.; Ergang, N. S.; Fan, W.; Karanikolos, G. N.; McCormick, A. V.; Penn, R. L.; Tsapatsis, M.; Stein, A. *Angew. Chem., Int. Ed.* **2008**, *47*, 9096–9099.

nucleation can occur. This precursor was used during each IHT step in our previous work, resulting in polycrystalline products that eventually adopted the shape of the pore space in the 3DOM carbon reactor (Scheme 1A: nucleation dominated reaction). When the dilute precursor, L, is used instead for each IHT cycle, nucleation is suppressed and crystal growth predominates, but at much slower rates, resulting in fewer but more regular zeolite crystals. Each of these crystals can grow through reactor windows and even through multiple adjacent macropores, forming a larger domain. (Note: In this paper, we define a "domain" as a region of interconnected solid product that can span multiple adjacent macropores and may be single crystalline or polycrystalline. We use the standard definition of a grain as an individual crystal.) Eventually, several of these relatively isotropic domains can merge together (Scheme 1B: growth dominant). To increase the number of initial nuclei, the reactor may be loaded with a precursor containing a high nutrient concentration in the first IHT cycle (H_1). Subsequent L cycles produce multiple well-faceted, discrete single crystals in each macropore, whose average sizes can be increased with further L cycles until these crystals finally merge into each other and the external shape becomes dictated by the macropore wall (Scheme 1C: shape development from irregular to faceted growth). Finally, the order of concentration schedules may be reversed. If an H cycle follows multiple L cycles, a new secondary population of smaller seeds is added to the existing domains, which can also be grown larger to manipulate the overall particle size distribution (Scheme 1D: secondary population). Size control and morphology control are thereby achieved through both confinement effects and precursor concentration effects.[27] These zeolite growth methods provide tools to design product morphologies tailored to specific applications. For example, when applied as building blocks for molecular sieve membranes, smaller, monodisperse, and suitably shaped zeolite particles can produce a thinner and better packed seed layer for membrane fabrication assisted by secondary growth, one of the promising methods to fabricate molecular sieve membranes.[8,28−31] Alternatively, extra empty void spaces introduced into zeolite crystals by a template (here the 3DOM carbon reactor) provide better accessibility of molecules to active sites in the zeolite particles, mitigating effects caused by diffusion limitations.[5,7,22,32−38]

Experimental Section

Reagents. The following chemicals were used without further purification. Resorcinol (99%), polydiallyldimethylammonium chloride (PDDA, MW = 100 000−200 000, 20 wt %), sodium polystyrenesulfonate (PSS, MW = 70 000, 30 wt %), tetrapropylammonium hydroxide (TPAOH, 1.0 M in H_2O), and tetraethyl orthosilicate (TEOS, 98%) were purchased from Aldrich. Sodium hydroxide (98%), nitric acid (68−70%), and hydrofluoric acid (48%) were obtained from Mallinckrodt Chemicals. Sodium carbonate (99.7%) and silicic acid (88.04%) were from J. T. Baker Chemical Co. Formaldehyde (37%) was purchased from Fisher Scientific and ethanol (200 proof) from Pharmco-Aaper. Deionized water with a resistivity of 18.2 MΩ·cm was used for all reactions.

3DOM Carbon and Polyelectrolyte Coatings. 3DOM carbon with ca. 350 nm macropores was prepared by infiltration of a resorcinol-formaldehyde precursor into PMMA colloidal crystals, followed by polymerization and carbonization according to a published procedure.[26,39] After oxidation and neutralization of the 3DOM carbon surface, multiple polyelectrolyte coatings were deposited as described previously[26] in the order PDDA, PSS, PDDA, PSS to produce a negatively charged surface, which can repel the silica precursor electrostatically.[40−43]

Hydrothermal Reactions. The silicalite-1 precursor solutions were prepared using the molar ratio 10 SiO_2 (from silicic acid)/2.4 TPAOH/0.87 NaOH/114 H_2O ("high nutrient concentration", H)[44] or 10 SiO_2 (from TEOS)/4.5 TPAOH/4750 H_2O ("low nutrient concentration", L).[45] 3DOM carbon was soaked in the precursor solutions and heated at 80 °C in closed, 130 mL Teflon bottles that were rotated for 2 days (for H) or 4 days (for L). After each seed growth step, the 3DOM carbon pieces were rinsed multiple times with deionized water, dried at room temperature, and reimmersed in fresh precursor solution. To study the shape development of zeolite particles, 3DOM carbon was first infiltrated with precursor H. After one IHT reaction, the 3DOM carbon monolith was mechanically polished to remove the more developed surface regions in which aggregates had already formed due to a concentration gradient across the monolith.[26,39] The remaining fraction contained isolated seeds and was used for subsequent infiltration with precursor L. When desired, products were calcined in flowing oxygen (0.5 L/min) for 6 h at 550 °C (heating rate 1 °C/min) to remove carbon and reveal the internal three-dimensional (3D) morphology of silicalite-1 products.

Characterization. Transmission electron microscopy (TEM) images were obtained using a FEI Tecnai G2 F30 TEM operating at 300 kV and collected using a CCD camera. Samples were crushed and supported on a holey carbon-coated copper grid (Ted Pella, Inc.) for the TEM investigation. Scanning electron microscopy (SEM) images were obtained with a JEOL 6700 microscope with an accelerating voltage of 5 kV and an applied current of 20 mA. All images were obtained without coating the samples except for the calcined samples, which were coated with 5 nm Pt.

Results and Discussion

Growth of Imprinted Single Crystals. Single crystal zeolite particles with imprinted macropores were prepared using multiple L_n steps. After cycle L_2, macropores contained sets of small, discrete zeolite particles with average diameters less than ca. 10 nm (Figure 1A and S1). Although these particles were attached to the carbon surfaces when they were imaged in the

(27) Barton, J. E.; Odom, T. W. *Nano Lett.* **2004**, *4*, 1525–1528.
(28) Lai, Z.; Bonilla, G.; Diaz, I.; Nery, J. G.; Sujaoti, K.; Amat, M. A.; Kokkoli, E.; Terasaki, O.; Thompson, R. W.; Tsapatsis, M.; Vlachos, D. G. *Science* **2003**, *300*, 456–460.
(29) Yoon, K. B. *Acc. Chem. Res.* **2007**, *40*, 29–40.
(30) Choi, J.; Ghosh, S.; Lai, Z.; Tsapatsis, M. *Angew. Chem., Int. Ed.* **2006**, *45*, 1154–1158.
(31) Gouzinis, A.; Tsapatsis, M. *Chem. Mater.* **1998**, *10*, 2497–2504.
(32) Jacobsen, C. J. H.; Madsen, C.; Houzvicka, J.; Schmidt, I.; Carlsson, A. *J. Am. Chem. Soc.* **2000**, *122*, 7116–7117.
(33) Janssen, A. H.; Schmidt, I.; Jacobsen, C. J. H.; Koster, A. J.; de Jong, K. P. *Microporous Mesoporous Mater.* **2003**, *65*, 59–75.
(34) Tao, Y.; Kanoh, H.; Kaneko, K. *J. Am. Chem. Soc.* **2003**, *125*, 6044–6045.
(35) Groen, J. C.; Bach, T.; Ziese, U.; Paulaime-van Donk, A. M.; de Jong, K. P.; Moulijn, J. A.; Pérez-Ramírez, J. *J. Am. Chem. Soc.* **2005**, *127*, 10792–10793.
(36) Choi, M.; Cho, H. S.; Srivastava, R.; Venkatesan, C.; Choi, D.-H.; Ryoo, R. *Nat. Mater.* **2006**, *5*, 718–723.
(37) Egeblad, K.; Christensen, C. H.; Kustova, M.; Christensen, C. H. *Chem. Mater.* **2008**, *20*, 946–960.
(38) Christensen, C. H.; Johannsen, K.; Schmidt, I.; Christensen, C. H. *J. Am. Chem. Soc.* **2003**, *125*, 13370–13371.
(39) Lee, K. T.; Lytle, J. C.; Ergang, N. S.; Oh, S. M.; Stein, A. *Adv. Funct. Mater.* **2005**, *15*, 547–556.
(40) Decher, G. *Science* **1997**, *277*, 1232–1237.
(41) Caruso, F. *Adv. Mater.* **2001**, *13*, 11–22.
(42) Wang, Z.; Ergang, N. S.; Al-Daous, M. A.; Stein, A. *Chem. Mater.* **2005**, *17*, 6805–6813.
(43) Nikolakis, V.; Tsapatsis, M.; Vlachos, D. G. *Langmuir* **2003**, *19*, 4619–4626.
(44) de Moor, P.-P. E. A.; Beelen, T. P. M.; van Santen, R. A. *J. Phys. Chem. B* **1999**, *103*, 1639–1650.
(45) Davis, T. M.; Drews, T. O.; Ramanan, H.; He, C.; Dong, J.; Schnablegger, H. A.; Katsoulakis, M.; Kokkoli, E.; McCormick, A. V.; Penn, R. L.; Tsapatsis, M. *Nat. Mater.* **2006**, *5*, 400–408.

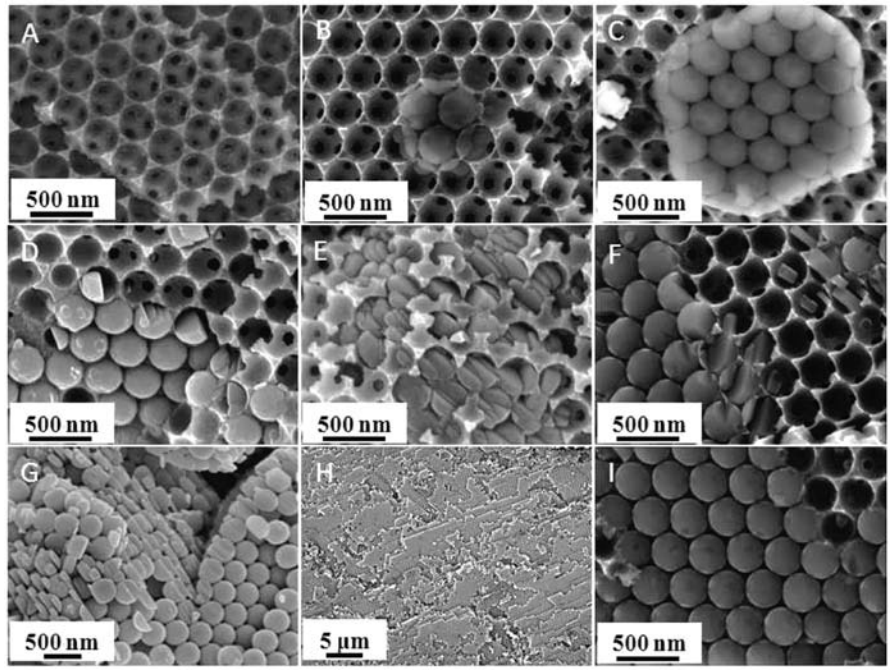

Figure 1. SEM images illustrating sequential single crystal growth using precursor L: (A−D) crystal domain growth in sequential IHT reactions after cycles L_2, L_3, L_5, and L_7, respectively, (E) different region after L_7, (F) after L_{11}, (G) calcined sample after L_{13}, (H) after L_{15}, (I) enlarged image of (H).

scanning electron microscope, they were probably detached from the walls before sample drying as a result of electrostatic repulsions between the silica particles and the negatively charged, outermost polyelectrolyte layers. In comparison, silicalite-1 particles formed by conventional, nonconfined hydrothermal synthesis from nutrient solution L were micrometer-sized and highly faceted (Figure S2A). After cycle L_3 in the confined reaction, domains were observed, in which a few adjacent macropores were completely filled with solid product (Figure 1B). These particles had smooth surfaces and overall rounded shapes. Some surface extrusions are visible where the particle had penetrated a window between neighboring macropores before the 3DOM carbon monolith was sectioned to obtain the SEM image. Cages surrounding these solid domains were nearly empty. This contrasts with the situation after cycle L_2, when small particles were evenly distributed throughout virtually all cages (Figure 1A and S1). With low nutrient concentrations and limited nutrient supply, the number of nuclei produced during the early stages (i.e., after cycles L_1 and L_2) is smaller and a fraction of these grow into larger crystals at the expense of smaller ones by typical Ostwald ripening processes. Under these conditions, most of the additional precursor added in subsequent steps appears to be consumed by the predominant seed crystals. This growth pattern is very different from that reported by us previously when a precursor with a high nutrient concentration was used.[26] Under those conditions, the greater nutrient supply ensured that all cages remained occupied by zeolite particles, which grew and produced polycrystalline spheres in relatively few H_n cycles. Eventually, their morphologies were determined by shape-confinement in the porous carbon reactor.

After L_5, larger domains of zeolite particles were observed, which were surrounded by empty macropores (Figure 1C). The exposed surface obtained after cross-sectioning the sample clearly shows the imprint of the 3DOM carbon template, which produced a smooth spherical morphology where the zeolite was in direct contact with the carbon walls. On the other hand, regions where the zeolite was not in direct contact with the carbon walls were frequently faceted. At this stage, the X-ray diffraction pattern of the composite showed clearly discernible lines for silicalite-1 (Figure S3).

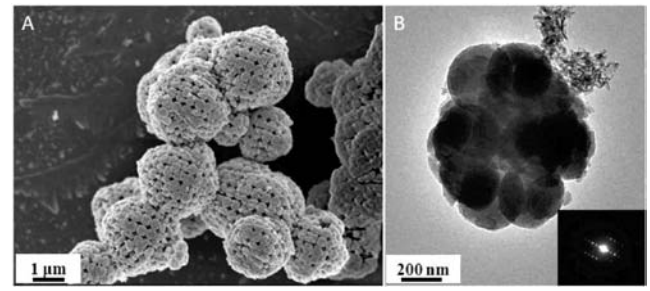

Figure 2. (A) SEM and (B) TEM images of the sample formed after L_5 and subsequent calcination. An SAED pattern of the particle shown in panel (B) is provided in the inset.

In an attempt to investigate the connectivity, overall shape, and crystallinity of the particle domains, the sample formed after L_5 was calcined to remove the carbon template. Rounded, robust domains of material with an opaline morphology and diameters of several micrometers are observed, many of which are interconnected (Figures 2A,B and S4). According to the selected area electron diffraction (SAED) patterns of the particle domain depicted in the TEM image (Figure 2B), this domain is a single crystal (Figure 2B, inset). Zeolite particles with this morphology may be of interest as hierarchical zeolite catalysts because they bring together the advantages of (1) short diffusion lengths within spheres molded by each macropore (e.g., 200−300 nm); (2) an open void structure that affords low mass transfer resistance; and (3) the ability to be treated from the standpoint of fluid mechanics as regular, micrometer-sized crystals, which offer lower pressure drop in packed beds and can be recovered from liquid mixtures or recirculated in fluidized beds.[5,7,22,32−37]

Subsequent L cycles resulted in a larger crystal population and further crystal growth. However, new structural features were also observed after L_7, including facets, steps, and

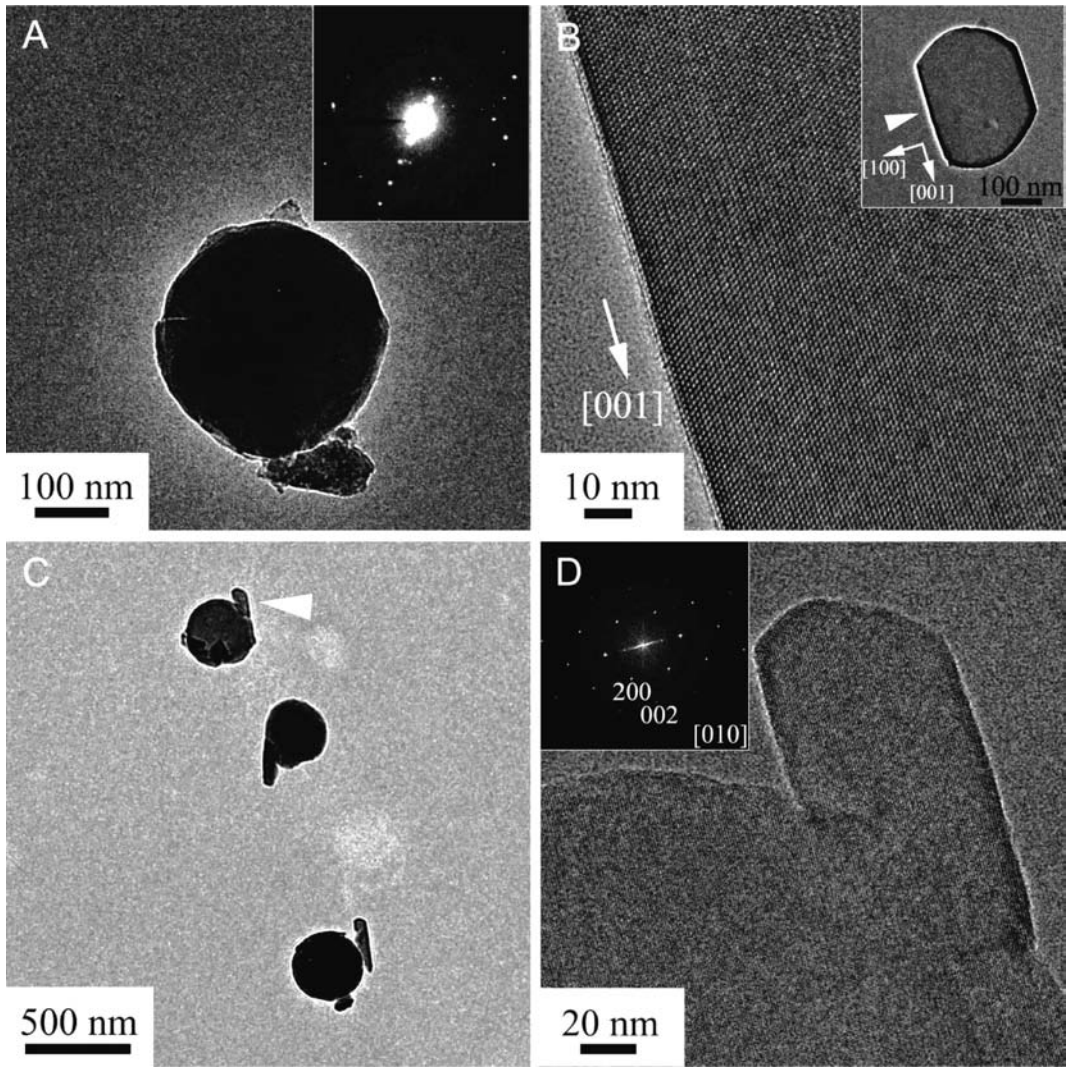

Figure 3. TEM images of various shaped zeolite crystals after cycle L_{11}: (A) a sphere templated by one macropore. The inset shows the corresponding selected area electron diffraction (SAED) pattern, confirming that the sphere is a single silicalite-1 crystal. (B) A representative crystal showing the influence of confinement on the characteristic coffin-like morphology of silicalite-1. The crystal is faceted along the *a*-planes. The facet marked by the white arrowhead is enlarged in the high resolution TEM image. (C) Three spheres with outgrowths. (D) High resolution image of the area marked by the white arrowhead in panel (C). The outgrowth follows the *c*-direction and its width is close to the size of windows in 3DOM carbon. The inset shows the corresponding fast-Fourier-transform (FFT) pattern of the imaged region, which is identical for the sphere and the outgrowth. A similar particle can be seen in the center of the SEM image shown in Figure 1F.

anisotropic shapes with plate-like (Figure 1D, 1E) and needle-like appearances (Figure 1F, top right area of image). These features predominate in the outside regions of a domain. In the internal regions, macropores are mostly filled with solid product, giving rise to spherical particles by shape confinement. As established above, many domains appear to be single crystals. Therefore, continued growth of such domains follows the typical growth directions of silicalite-1 crystals, as long as the domain remains isolated from other domains. The steps and plate-like shapes result from crystal faces that are exposed as the crystal grows under limited nutrient supply. If additional nutrient can reach these sites, they eventually fill in until the crystal reaches the carbon walls. If nutrient supply is cut off earlier, the steps and edges remain in the product. The needle-like structures may result from growth of the crystals through a macropore window. The SEM image of the calcined product after cycle L_{13} (Figure 1G) shows relatively smooth spheres in the interior of a domain, with more faceted features on the periphery. This particular image reveals the merging of two adjacent domains, which nucleated from two separate centers. In this "frustrated region", competition between crystallization and growth of the adjacent domains is likely to influence the surface features near the interface. Nearly all of the 3DOM carbon template is filled with single crystal zeolite particles after L_{15}, showing a mixture of crystal domains at various growth stages (Figure 1H and I). Spheres can be isolated by calcination and extended sonication.[26]

For a detailed investigation of crystallographic features in these templated zeolite particles, the sample obtained after L_{11} was analyzed by high-resolution TEM. Figure 3A shows a TEM image of a particle that had filled a whole macropore and therefore took on the spherical shape of the macropore. The corresponding SAED pattern confirms that this zeolite sphere consists of a single crystal. This is in contrast to the polycrystalline spheres obtained with more concentrated silica precursors.[26] The inset in Figure 3B shows another particle with a morphology that combines the characteristic hexagonal prismatic shape of silicalite-1 with more rounded edges. The longest dimension is along *c* (i.e., the preferred growth direction that is

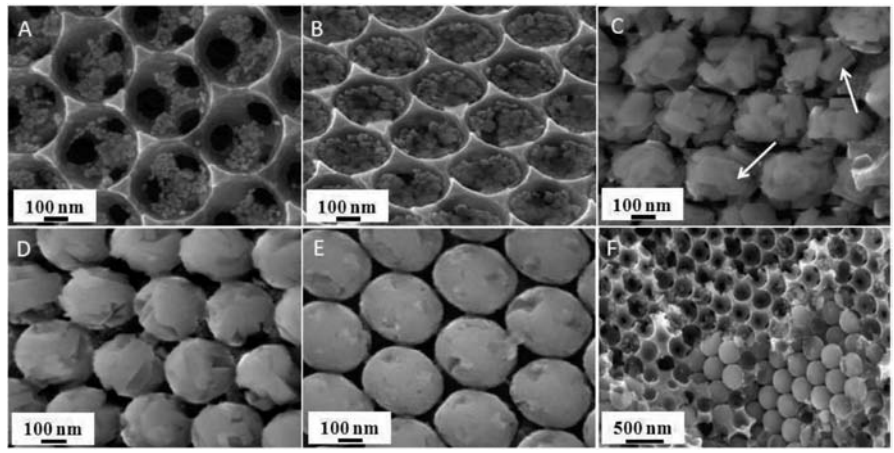

Figure 4. SEM images illustrating the shape development of zeolite particles during programmed growth with multiple concentration schedules: (A) product obtained after H_1. (B) Product obtained after a H_1L_1. (C) Product after H_1L_2, clearly showing faceted, coffin-like crystals. The white arrows point at twinned crystals. (D) Product after H_1L_3 and (E) product after H_1L_4. At these stages, crystals aggregate and growth becomes limited by confinement inside the 3DOM carbon monolith. (F) A secondary population of irregular zeolite particles is produced after applying precursor H following six L cycles (L_6H_1). (See also the Supporting Information, Figure S7.)

also observed in nonconfined syntheses) and the particle is faceted along *a*-planes. The {101}-type planes of the usual prismatic shape have been smoothed out by confinement in the 3DOM carbon template. The sharp edge planes on both sides suggest that anisotropic growth inside macropores first produces faceted particles and eventually fills the macropores: when one macropore is not fully occupied, the anisotropic growth follows the *c*-direction until the pore is filled, and it either becomes rounded by wall confinement or continues to grow through a pore window. Not surprisingly, the major growth direction is influenced by the internal structure in each crystal, not by the 3DOM carbon template. For example, the images in Figures 1F and 3C,D show finger-like outgrowths from spheres that are not perpendicular to the sphere surface (i.e., the window direction), but instead follow the *c*-growth direction. Crystal growth clearly occurred through a window in these cases, but the direction of fastest growth was not changed by the carbon walls. This observation is in contrast to a recent report of crystal orientation of glycine inside nanoporous polystyrene-poly(dimethyl acrylamide), where the crystal size was comparable to the 20 nm diameter of the one-dimensional pores of the polymer template and the fastest growth direction was parallel to the axis of the cylindrical mesopores.[46] In our case, the pores are larger and 3D interconnected.

Shape Development of Discrete Zeolite Particles. In our previous work, which employed only precursor H, a large number of seeds was produced in the initial IHT step and grew into irregular particles and then polycrystalline spheres after multiple cycles.[26] In contrast, using a sequence of an initial H_1 step and subsequent L cycles made it possible to produce small, well-faceted zeolite crystals. Reaction conditions favored nucleation during cycle H_1 and produced irregular zeolite particles ca. 10−40 nm in length (average length 24.5 ± 5.4 nm) throughout most of the 3DOM carbon monolith (Figure 4A), that is, slightly smaller than after an identical hydrothermal reaction without confinement (average diameter 67.7 ± 8.7 nm, Figure S2B). Outermost layers of the monolith containing more completely filled macropores[26] were removed by mechanical polishing before continuing with L_n cycles. The new conditions

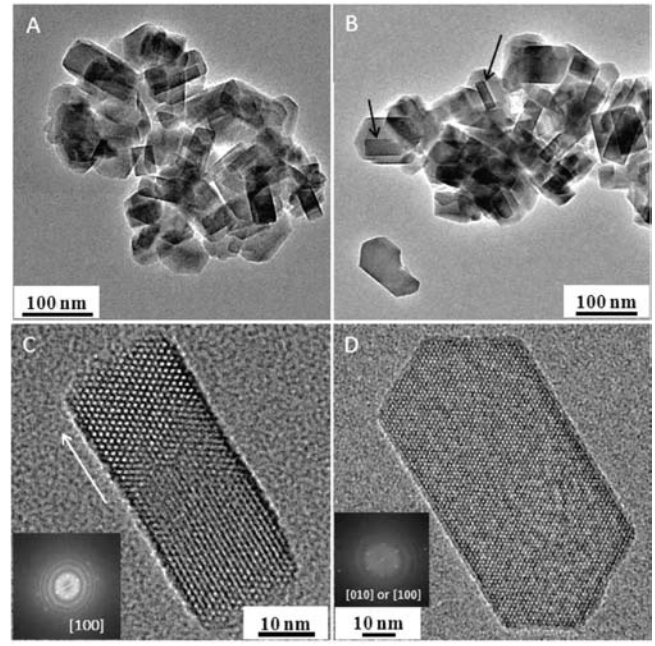

Figure 5. TEM images illustrating the shapes, pore structures, and crystallinity of the faceted, brick-like, and coffin-like products shown in Figure 4B,C: (A and B) low magnification images of the products obtained after cycles H_1L_1 and H_1L_2, respectively, (C and D) higher magnification images of crystals obtained after cycles H_1L_1 and H_1L_2, respectively. The black arrows in panel (B) indicate twinned structures and the white arrow in panel (C) indicates the *c*-orientation. FFT patterns of the TEM images in panels(C) and (D) are presented in the insets.

favored crystal growth from the original nuclei. During cycles H_1L_1 and H_1L_2, continuous growth produced highly crystalline, well-faceted, discrete zeolite particles whose average sizes increased with each cycle (Figures 4B,C and 5). A distribution of sizes resulted, which could be attributed partly to the size variation of the parent seeds produced during cycle H_1 (see Supporting Information, Figure S5). After H_1L_1, most of the smaller crystallites appeared to be brick-shaped (see Figure 5A,C), whereas the fraction of coffin-shaped particles (a common morphology for an MFI-type zeolite, Figure 5D) increased after H_1L_2 (Figure 5B). We also observed several twinned structures (indicated by arrows in Figures 4C and 5B). The morphological

(46) Hamilton, B. D.; Weissbuch, I.; Lahav, M.; Hillmyer, M. A.; Ward, M. D. *J. Am. Chem. Soc.* **2009**, *131*, 2588–2596.

development of zeolite particles from irregular to well-faceted is a consequence of the lower precursor concentration, which introduces fewer seed particles and instead provides a low level of nutrients for slow hydrothermal crystal growth. Rectangular and coffin-shaped zeolite particles with lengths less than 100 nm have recently been reported as products of conventional hydrothermal reactions[12] and faceted silicalite-1 nanocrystals ca. 100 nm × 40 nm × 200 nm in size as products obtained in an anionic microemulsion as a soft template.[47] The thickness of the faceted zeolite particles produced here is much smaller than 100 nm, so that these well-faceted zeolite particles may be suitable as building blocks for seed layers of molecular sieve membranes prepared by secondary growth methods.[8,28−31] They can be isolated by calcination and sonication (Figure S6).

After additional L cycles, faceted zeolite particles grew into each other, especially in the periphery region of the 3DOM carbon monolith (Figure 4D, after H_1L_3). Eventually, intergrowth of these crystals and confinement by the carbon walls produced rounded particles with relatively smooth surfaces (Figure 4E, after H_1L_4). These merging and confinement effects are similar to our previous observations for polycrystalline growth of zeolite spheres under confinement in 3DOM carbon (when a precursor with high nutrient concentration was used throughout all IHT cycles), although in the present case, the spheres contain fewer and larger crystal grains.[26]

Secondary Population Growth. By altering the sequence of H and L cycles, it is also possible to produce multiple populations of zeolite particles with different size distributions. As we have seen, introduction of precursor solution H favors nucleation of new seeds. We have already demonstrated this when the high concentration precursor was used in the first IHT cycle. However, the nucleation effect is also observed when a precursor H is used at a later cycle, following a series of L cycles (i.e., growth-dominant conditions). Figure 4F shows an SEM image of a product obtained after six L cycles and one subsequent H cycle (L_6H_1, see also the enlarged Figure S7 in the Supporting Information). Because of the nucleation dominant conditions created by the high nutrient content in solution, a second population of small, irregular zeolite particles formed in the available spaces between larger domains. This behavior shows that, even in the presence of crystals in the 3DOM carbon reactor, the H mixture nucleates fast enough to start a new population. The effect may be attributed to the presence of the 3DOM carbon matrix which slows down diffusion of dissolved species and small nanoparticles, while eliminating diffusion of the existing zeolite crystals and, hence, creating isolated regions with conditions very similar to those in H mixtures without preexisting crystals. Thus, judicious scheduling of IHT cycles with conditions that favor either nucleation or growth permits some control over particle size distribution in the zeolite product. Controlled mixtures of particle sizes would be of interest for preparing densely packed seed layers for zeolite membranes by potentially filling spaces between layers of larger particles with smaller particles.

Conclusion

We have demonstrated that varying the sequence of precursor concentrations in multistep hydrothermal reactions under confinement permits control over morphology, grain size, density of grain boundaries, and particle size of the hydrothermal products, specifically the zeolite silicalite-1. Depending on the relative magnitudes of nucleation and growth rates, development of the crystal grain shape from irregular to faceted is possible and controlled syntheses of single crystal or polycrystalline zeolite particles can be achieved. Nucleation dominant conditions (i.e., high precursor concentrations) result in polycrystalline zeolite particles, whereas growth dominant conditions lead to larger single crystals. Further research will be necessary to determine nutrient concentrations that would provide a transition from growth-to-nucleation dominant. If the zeolite crystals remain smaller than the size of the confinement space, they can be isolated as discrete particles with morphologies defined by their crystal structure. If, on the other hand, the crystals are permitted to grow without additional nucleation, they can extend through the windows of multiple reactor cages and are eventually shaped by the host (the 3DOM carbon reactor) to form spheres or close-packed sphere arrays. The domains can be isolated by calcination, producing single crystalline zeolite particles with hierarchical porosity, created by the structure-directing agent (micropores) and by the reactor walls that act as a hard template (mesopores/macropores). These particles combine features of nanoparticles and macroscopic objects. Although similar single crystalline hierarchical zeolites have previously been prepared in much smaller, 10−40 nm, mesopores,[25] a very different reaction, steam-assisted crystallization, was employed in that case. It is therefore notable that single crystallinity is maintained through multiple sets of much larger, 350 nm pores of the 3DOM carbon reactors when hydrothermal reactions are used. A secondary population with smaller particle sizes could be introduced to existing zeolite crystals by application of a nucleation step following multiple growth steps.

Depending on their morphologies, the products from these reactions are interesting for different applications. 3DOM carbon-imprinted zeolite particles may be used as a hierarchical zeolite catalyst, and well-faceted, coffin-shaped zeolite particles with average lengths less than 100 nm are suitable as seed layers for syntheses of molecular sieve membranes. The concept of scheduling nucleation and growth-dominant cycles in multistep hydrothermal reactions using confinement may also be extended to other hydrothermal reactions (e.g., synthesis of other zeolites) in future research.

Acknowledgment. Funding was provided by the NSF (mainly by CMMI-0707610 and in parts by DMR-0704312, DMR-0212302 and CBET-0522518). Parts of this work were carried out in the Institute of Technology Characterization Facility, University of Minnesota, which receives partial support from NSF through the NNIN program and has received capital equipment funding from the NSF through the MRSEC, ERC, and MRI programs.

Supporting Information Available: Enlargements of the SEM images in Figures 1A and 4F, SEM images of products obtained by conventional hydrothermal reactions, X-ray diffraction patterns of selected products, a low magnification SEM image of the calcined sample after cycle L_5, a histogram of the particle size distribution of zeolite seeds produced after cycle H_1 and an SEM image of isolated faceted particles. This material is available free of charge via the Internet at http://pubs.acs.org.

(47) Lee, S.; Carr, C. S.; Shantz, D. F. *Langmuir* **2005**, *21*, 12031–12036.

JA904466V